Two-center effect on low-energy electron emission in collisions of 1-MeV/u bare ions with atomic hydrogen, molecular hydrogen, and helium: II. H_2 and He

Lokesh C. Tribedi,[1,*] P. Richard,[2] L. Gulyás,[3] and M. E. Rudd[4]
[1]*Tata Institute of Fundamental Research, Homi Bhabha Road, Colaba, Mumbai-400005, India*
[2]*J.R. Macdonald Laboratory, Department of Physics, Kansas State University, Manhattan, Kansas 66506-2601*
[3]*Institute of Nuclear Research of the Hungarian Academy of Science (ATOMKI), P.O. Box 51, H-4001 Debrecen, Hungary*
[4]*Department of Physics and Astronomy, University of Nebraska, Lincoln, Nebraska 68588-0111*
(Received 25 September 2000; published 17 May 2001)

We have studied the energy and angular distributions of low-energy electron emission in collisions of bare carbon ions of 1-MeV/u energy with He and H_2 targets. The double-differential cross sections (DDCS's) are measured for electrons with energies between 0.5 and 300 eV emitted within an angular range of 15° to 160°. The large forward-backward asymmetry observed in the angular distributions is explained in terms of the two-center effect. Single differential cross sections (SDCS's) and total cross sections are also derived by integrating the DDCS's over emission angles and energies. The data are compared with different theoretical calculations based on the first Born, CDW (continuum-distorted-wave), and CDW-EIS (eikonal-initial-state) approximations. The angular distributions of DDCS's and SDCS's are shown to deviate largely from the predictions of the B1 calculations, and are in much better agreement with both the continuum distorted-wave models. The CDW approximation provides a better agreement with the data compared to the CDW-EIS approximation, especially at higher electron energies. The total ionization cross sections for all three targets are shown to follow a scaling rule approximately.

DOI: 10.1103/PhysRevA.63.062724 PACS number(s): 34.50.Fa

I. INTRODUCTION

Collisions between bare ions and helium atoms can provide important information on the ionization dynamics beyond the case for atomic hydrogen. Helium is the simplest two-electron system in which to study ion-atom collisions, and can be used as a prototype for describing ionization of many electron systems. The measurements of the energy and angular distributions of electron double-differential cross sections (DDCS's) in the ionization of He by different high-energy (1.8–5 MeV/u) bare ions have been reported recently [1–3]. Different approximate models have also been developed to specify the wave function to be used either in first Born or the continuum-distorted-wave (CDW) calculations. Two such distorted-wave calculations are commonly used in studies of ionization, namely, the CDW-EIS (eikonal initial state) [4,5] and CDW calculations. As discussed in paper I, the main difference between the CDW-EIS and CDW approximations lies in the forms of distortions applied in the initial channel. The former accounts for the distortion in the initial channel by using an eikonal phase, while the latter, similar to the final channel, uses a continuum distortion. The eikonal phase corresponds to the asymptotic behavior of the continuum distortion at asymptotic distances, thereby reducing the role of the two-center character of the distorted-wave functions on the electron emission. However, a stringent test to these models can be provided by comparing them against the measured energy and angular distributions electron DDCS's. Moreover for two-electron or multielectron atoms, it is quite common to use a H-like wave function with an effective atomic number Z_{eff} derived from the binding energy. The CDW-EIS model was recently improved [6] to include realistic or numerical Hartree-Fock-Slater (HFS) wave functions for an active electron in the initial and final states. It was also demonstrated that the inclusion of such wave functions in the calculations improves the agreement with the experimental data [2,3] at higher energies.

As discussed in paper I, the two-center effect (TCE) can be studied by measuring the forward-backward angular asymmetry in low-energy electron emission using conventional electron spectroscopic techniques. The recoil-ion-momentum spectroscopy (RIMS) technique, using cold targets, was also used recently to study the two-center effects and its influences on the emission of low-energy electrons and recoil ions [7]. The relation between electron spectroscopy and RIMS was also addressed recently [8–10] in order to study the ion-atom ionization mechanism. The observed shift in the recoil-ion and electron longitudinal momentum distributions in the opposite directions is believed to be associated with such two-center effects [11], which is shown to be stronger with higher values of the perturbation strength $S_p = Z_p/v_p$, where Z_p and v_p are the atomic number and velocity of the projectile, respectively. A large shift, and hence a large post-collision interaction, is observed for $S_p = 2.0$, whereas a negligible shift in the electron and recoil-ion longitudinal distributions is noted in the case of much smaller values of $S_p (= 0.6)$ [8]. However, in spite of a negligible shift in the momentum distributions [10], a large forward-backward asymmetry was observed in the electron emission for $C^{6+} + He$ with S_p quite small, i.e., 0.6 [3] and 0.4 [2]. The goal of the present measurement is to explore the TCE by measuring the forward-backward asymmetry in the angular distribution of low-energy electron emission in fast ion-atom collisions with He and H_2, for which the perturbation strength is nearly 1.0 ($S_p = 0.94$).

*Email address: lokesh@tifr.res.in

Molecular hydrogen is also a two-electron system. The investigation of the ionization mechanism of H_2 in heavy-ion collisions can serve as a basis for understanding the ionization of more complex molecules in such collisions. Molecular hydrogen data are not only required for deriving the cross sections for atomic H [see Eq. (1) in paper I], but are also important to test the model calculations, which are used in an attempt to explain the ionic collision with this simple molecule with the help of the independent-particle approximation. The experimental data and model calculations for the interaction of ions with molecular hydrogen are also required to gain a knowledge of many other physical systems in nature, including the astrophysical and laboratory plasmas. Our theoretical treatment is based on an independent-electron model, which ignores electron-electron interaction. Furthermore, we simplify the molecular hydrogen target as an effective one-electron hydrogenic target with charge $Z_{eff}=1.064$, where $Z_{eff}^2/2$ gives rise to the ionization potential of H_2. Such a simplification of the multielectronic targets relies on the fact that the ionization potential has proved to be one of the most crucial parameters in accounting the main features of ionization process. The sensitivity of emission of extremely slow electrons to the use of different effective charges warrants more elaborate calculations using molecular wave functions in the future. The testing of molecular target effects in the single ionization of H_2 was carried out extensively in the past [12]. At high collision energies, total single-ionization cross sections for H_2 target are essentially twice the atomic ionization cross sections. To our knowledge, such calculations have not been done for double-differential cross sections. The total cross section of dissociative ionization and double ionization is only about 5–10 % of the total ionization cross section, for the present collision systems [13,14] and therefore single ionization is the main reaction channel.

II. EXPERIMENTAL DETAIL

The experimental details were already described in paper I, and hence will not be discussed here. All the measurements were carried out at the van de Graaff accelerator facility in the J.R. Macdonald Laboratory at Kansas State University (KSU). The same hemispherical analyzer was used in the experiment to measure the angular distributions of the low-energy electron emission. The angular distributions of electron DDCS's are measured in small angular steps. The electrons with energies between 0.5 and 300 eV are detected at different angles, namely, 15°, 20°, 30°, 45°, 50°, 60°, 70°, 80°, 90°, 95°, 105°, 120°, 135°, and 160° for H_2 and He targets. The spectrum was taken with and without the target gas in the chamber. The spectrum collected without gas was used to subtract the background, which mainly arises due to slit scattering and the beam interaction with the residual gas atoms. The chamber was flooded with He or H_2 gas at a low pressure (0.1–0.15 mTorr) for the low-energy scan (0.5–50 eV). The low pressure was required to minimize the rescattering of the low-energy electrons from the gas molecules. The data were corrected to account for the loss due to the scattering of low-energy electrons from the target gas while moving toward the spectrometer entrance. The correction factor was found to be less than 5% [15] and 10% for He and H_2 [16], respectively. However, for higher-energy (30–300 eV) scans a higher gas pressure (0.3–0.45 mTorr) was used. The pressure dependence was also studied to ascertain the region for single-collision conditions. To achieve a ''static'' gas pressure in the chamber, a paddle was used on the top of the pump to reduce the load on the pump.

To put the measured electron yields on an absolute scale, we measured, at different angles, the electron energy spectrum from the ionization of He in a collision with 1.5-MeV protons for which the cross section data are known [17]. From these measurements a normalization factor was obtained which was energy and angle independent within about 7%.

The statistical error was low ($<5-10\,\%$) except for the extreme backward angles for which the cross sections are very low. For these angles ($\theta_e \geqslant 120°$) the statistical error was 5–15 %. The absolute errors in the cross sections, which were typically 25–30 % between 5 and 100 eV, resulted from the normalization procedure, the counting statistics, and the background subtraction. For electron energies below 5 eV and above 100 eV the absolute errors could be as large as 30–50 %. The lowest-energy electrons easily could be deflected by stray fields, and may cause additional systematic errors. Extreme precautions were taken to ensure the cleanliness inside the scattering chamber to remove any source of electrostatic fields. The magnetic field was reduced to about 5 mG or less by using μ-metal shielding and an external coil. These were required to detect the lowest-energy electrons (<1 eV). Above 100 eV statistical errors were relatively large because of the substantial background and low ionization cross sections, especially for the backward angles. A slight fall in the cross sections below 1 eV, for a few angles, could be due to the stray fields.

III. RESULTS AND DISCUSSION

The results are discussed in three sections. First we present the energy distributions of the electron DDCS's at different angles. In Sec. V, we display the angular distributions of the electrons having different energies. The single-differential distributions derived from the DDCS's are also discussed. The total cross sections derived for all three targets, along with our recent data at higher energies, are then shown to follow a scaling rule suggested by Wu *et al.* [18].

IV. ENERGY DISTRIBUTIONS OF DDCS'S

In Fig. 1 we display the electron energy distributions of the measured double-differential cross sections for several forward and backward angles. The measurements are compared to the three theoretical calculations. In the case of emission at 30°, the first Born (B1) calculations in general fall much below the experimental data. The deviation increases gradually above 10 eV, and underestimates the experimental data by a factor of 6 at 300 eV. The post-collision interaction between the projectile and the electrons largely influences the emission in the extreme forward angles. The lowest-energy electrons are affected less, since they are pro-

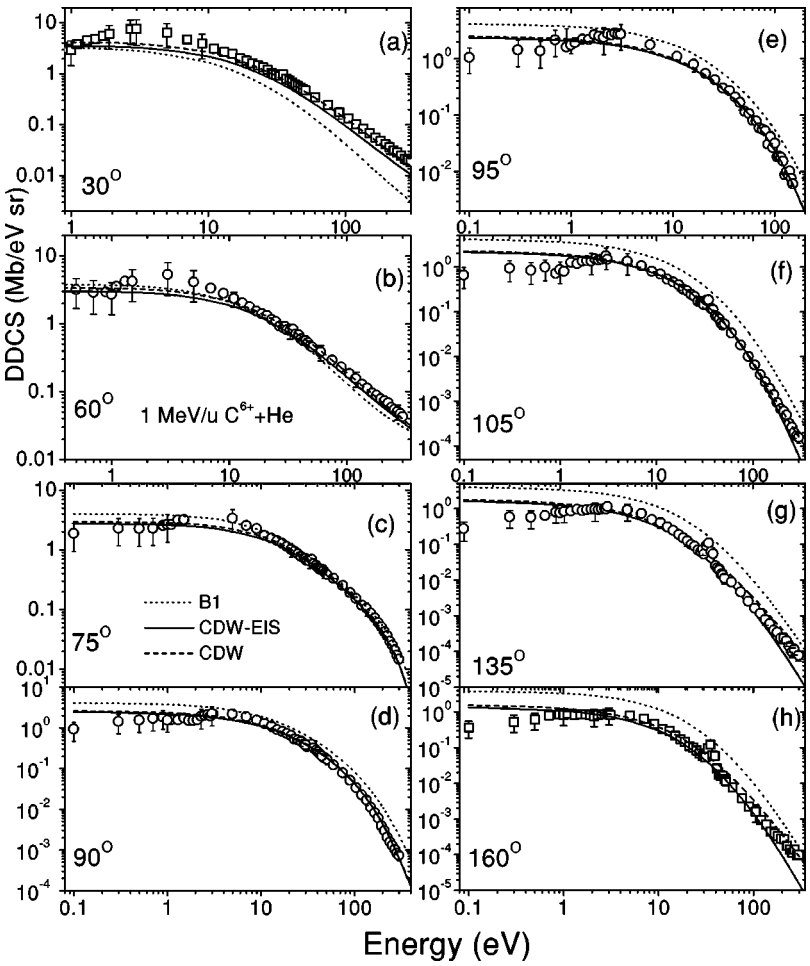

FIG. 1. The double-differential cross sections of electron emission for a He target. The data in different panels correspond to different emission angles as indicated. The CDW-EIS (solid line), CDW (dashed line), and B1 (dotted line) calculations are also shown.

duced in large impact parameter collisions, and hence the large deviation from the B1 calculations with higher energy electrons are observed. The CDW-EIS model, on the other hand, explains the data much better than the B1 model, but still underestimates the cross section by $\sim 25-50\,\%$ throughout the energy. The CDW model gives a better agreement, and the calculations reproduce the data over the entire energy range. In the case of slightly larger forward angles, i.e., for 60°, all three calculations reproduce the data set very well. The B1 calculations, however, show some deviations above 50 eV. Both of the distorted-wave calculations reproduce extremely well the data measured at 90° over the entire energy range, i.e., between 0.5 and 300 eV. The B1 calculations overestimate the DDCS's over the whole energy range from 25 to 250%. The behavior remains almost the same in the case of small backward angles such as 95°. At 105° and 135° the B1 calculations overestimate the data by a factor of 2–4. Both the CDW and CDW-EIS calculations reproduce the absolute values and the energy dependence quite well, except for higher-energy electrons for which the CDW-EIS calculations fall below the data. In fact, both the continuum distorted-wave calculations give almost the same cross sections below 100 eV for 105° and below 50 eV for 135° above which they start differing from each other, and CDW calculations closely follow the data. The difference between these two calculations becomes quite large at 300 eV, for which the CDW model predicts factors of 3 and 6 larger values compared to the CDW-EIS calculations at 150° and 135°, respectively. A very similar trend is observed in the case of the extremely large angle of 160°, as shown in Fig. 1(h).

Figure 2 shows the similar energy distributions of the DDCS's for H_2 targets. At small forward angles 15° (and 45°), the deviation of the B1 calculations from the data above 5 eV is obvious. The B1 results fall well below the data indicating a large influence due to the two-center effect on the forward-electron emission. The CDW-EIS results also fall below the observed cross sections whereas the CDW results show a much better agreement. At 80° and 90° there is a better agreement among all three calculations and the measured DDCS's. At large backward angles 135° and 160°, the CDW-EIS model reproduces the data between 2 and 100 eV, beyond which the calculations start falling below the measured trend while the CDW model remains good even up to 300 eV. The first Born calculations, however, overestimate the measured DDCS's up to about 100 eV, above which the calculations seem to be in good agreement. It may be noted that the low-energy part of the spectra at all the angles are not reproduced by any of the theories used here, whereas, in the case of the He target, the same calculations provided a better agreement with the data at lower energies, at least in the forward angles. Apart from the low-energy data, the spectra at all the angles are much better reproduced in the case of the He target compared to that for H_2. This

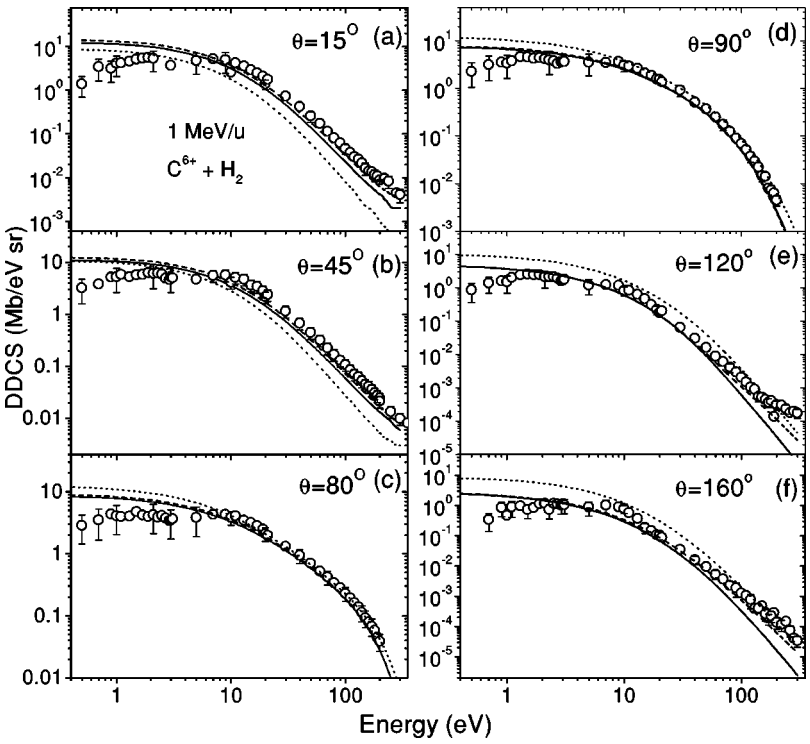

FIG. 2. The double-differential cross sections of electron emission for H_2 targets. The lines have the same meaning as in Fig. 1.

may reflect the inadequacy of the approximate representation of the H_2 target in terms of the independent-electron approximation, especially for the low-energy electrons.

V. ANGULAR DISTRIBUTIONS OF ELECTRON DDCS'S

In Fig. 3 we show the angular distributions of the DDCS's at some fixed energies for the He target. The data for He targets also can be found in Table I. The electron energies are chosen to be 10, 40, 100, 200, 240, and 300 eV (see Fig. 3). The distributions at all the energies shown fall sharply above 60°. At small forward angles the distributions increase slowly with decreasing angle, or remain almost flat. At higher electron energies, however, a humplike structure is observed around 60°. This behavior is slightly different from the earlier observations of a sharp peaking at around 70°–75° at higher-energy ($v=10$–15 a.u.) collisions of $C^{6+}+He$ [3,2]. In the present collisions, the velocity being lower ($v=6.35$ a.u.), the projectiles have enough time to drag the low-energy electrons into a small forward cone.

As mentioned in paper I, the peaks in the angular distributions are due to the binary collisions (commonly known as the binary encounter approximation) between projectiles and electrons. The widths of the peaks are due to the initial momentum distributions of the electrons. In the case of He, the Compton profile being wider compared to that for H or H_2,

TABLE I. Some of the measured electron DDCS's (in Mb/eV sr) for 1-MeV/u $C^{6+}+He$ at some selected energies (ε) and emission angles (θ). Typical errors are about 25% except for $\varepsilon \leqslant 5$ eV, for which the errors could be 40–50 %. For backward angles the uncertainty is large (about 30–40 %) for higher-energy ($\varepsilon \geqslant 100$ eV) electrons.

θ \ ε	5 eV	10 eV	40 eV	100 eV	150 eV	200 eV	240 eV	300 eV
15°	7.3	4.60	0.76	0.162	0.0743	0.104	0.0311	0.0220
30°	6.51	3.6	0.71	0.147	0.0686	0.0396	0.0283	0.0184
45°	6.12	3.45	0.68	0.156	0.080	0.0475	0.0341	0.0239
60°	4.11	2.58	0.64	0.200	0.113	0.0763	0.0583	0.0427
75°	3.38	2.00	0.53	0.165	0.087	0.045	0.029	0.0147
85°	2.8	1.51	0.37	0.082	0.0301	–	–	–
90°	2.19	1.4	0.27	0.040	0.0112	0.0036	0.00156	7.29E-4
95°	2.06	1.25	0.223	0.031	–	–	–	
105°	1.32	0.74	0.096	0.0076	0.00193	6.36E-4	3.16E-4	1.55E-4
120°	1.14	0.58	0.054	0.0039	8.59E-4	3.27E-4	2.01E-4	1.31E-4
135°	0.91	0.445	0.038	0.0019	5.97E-4	2.36E-4	1.36E-4	7.67E-5
160°	0.80	0.41	0.043	0.00180	4.47E-4	2.78E-4	1.39E-4	1.01E-4

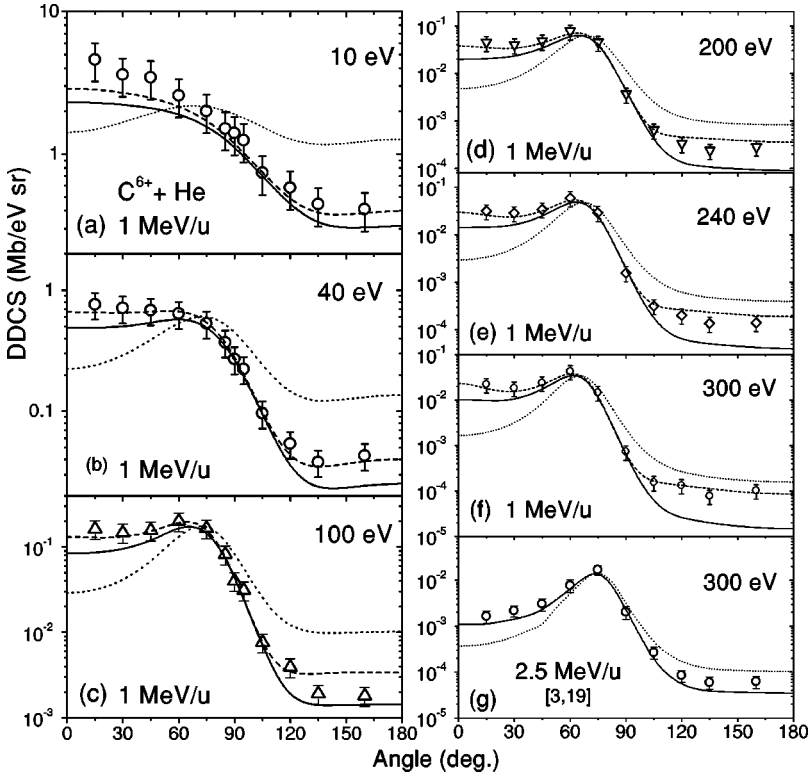

FIG. 3. The angular distributions of electron DDCS's for He targets measured at different electron energies as indicated in different panels. The different calculations are also shown by solid (CDW-EIS model), dashed (CDW model), and dotted (B1 model) lines. (a)–(f) 1 MeV/u C^{6+} + He. (g) 2.5-MeV/u C^{6+} + He. The data for 300 eV in (g) are taken from Ref. [3] (see Ref. [19]).

the peaks are relatively broader. The results from the distorted-wave theories show that the effects of the TCE appears mostly at the tails of the peaks by drastically changing the asymmetry character. The large asymmetry between the forward and backward emission is obvious, since the DDCS in the extreme forward angles is larger than that for the most backward angles by a factor of 12 at 10 eV, and by a factor of 90 at 100 eV. This factor increases to about 220 at 300 eV, indicating the existence of a strong two-center effect. The B1 calculations, which do not include the two-center effects, predict a much more symmetric distribution about the peak. For example, according to the B1 calculations, the ratio between the DDCS's at 15° and 160° is found to be about 1.2 at 10 eV, 3.1 at 100 eV, and to increase to only about 12 at 300 eV. Both continuum-distorted-wave calculations reproduce the angular asymmetry much better than the B1 calculations although one finds small discrepancies. The CDW-EIS results give the best agreement between 60° and 105°, and fall below the data at small forward and large backward angles. For example, at 10 eV the CDW-EIS results fall below the data by about 40–50 % at the lowest angles, and by about 25% at large backward angles. A similar deviation is found at forward angles for higher energies, but at backward angles the deviation is larger. The calculations underestimate the data at backward angles by a factor of 1.5 at 40 eV, and this deviation increases to factors of about 3.0 at 200 eV and about 6.0 at 300 eV. The CDW calculations, on the other hand, reproduce the forward-backward angular asymmetry and the absolute magnitudes much better at all the energies. In fact, the calculated cross sections pass through almost all the data points within error bars. It may indicate that the CDW model is more suitable to describe the TCE in heavy ion-atom collisions.

It may be noted that at a higher beam energy the CDW-EIS model gives better agreement with the DDCS data [3] for the backward angles for high-energy electrons. For example, in Fig. 3(g) we display the angular distributions of DDCS's of electrons emitted with 300-eV energy in a collision of 2.5 MeV/u C^{6+} + He (taken from Ref. [3], and corrected for a few typographical mistakes [19]) (see Table II). It is obvious that the CDW-EIS results fall below the data at large backward angles only by a factor of about 1.5–1.7, which is much smaller than that for 1-MeV/u collisions [see Fig. 3(f)].

The angular distributions of the DDCS's in the case of the H_2 target are shown in Fig. 4 for different electron energies (see Table III). It may be noted that the distributions gradually take the shape of a peaklike structure around 70° with higher energies, and this behavior is quite different from that observed for He targets, in which flat distributions in the forward angles are observed instead. This difference arises from the difference in the Compton profiles between H_2 and He, which affects the width of the binary peaks. Also, the deviations from the theories are larger for H_2 than for He or H targets (see paper I). The B1 calculations deviate strongly

TABLE II. The corrected [19] double-differential cross sections (in units of Mb/eV sr) for 2.5-MeV/u C^{6+} + He at a few energies and two backward angles, taken from Ref. [3].

$\varepsilon\downarrow$, $\theta\rightarrow$	105°	160°
210 eV	9.50E-4	1.99E-4
240 eV	5.60E-4	1.33E-4
270 eV	3.22E-4	1.06E-4
300 eV	2.68E-4	6.23E-5

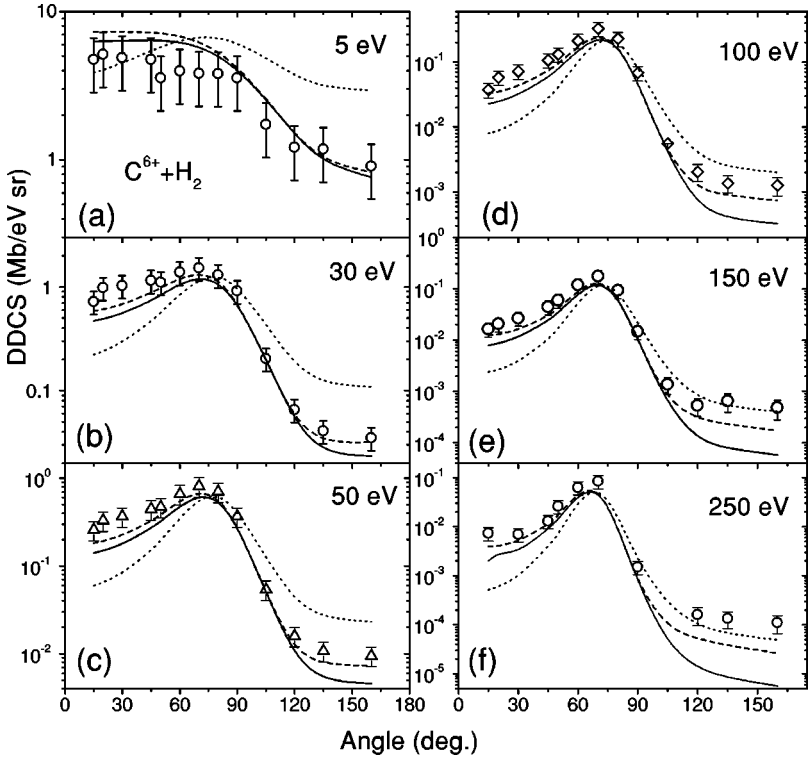

FIG. 4. The angular distributions of electron DDCS's for 1-MeV/u $C^{6+}+H_2$ measured at different electron energies as indicated in different panels. The different calculations are also shown by solid (CDW-EIS model), dashed (CDW model), and dotted (B1 model) lines.

from the measured data at forward as well as backward angles. Of course, for higher-energy electrons the B1 calculations come closer to the data at large backward angles. For 30, 50, and 100 eV, both the CDW-EIS and CDW calculations fall below the data at small angles and at large backward angles. The CDW model, however, continues to give a better agreement in backward angles, and shows a slight deviation from the data in small forward angles. The deviations in both distorted-wave calculations from the data are larger for H_2 targets than for He targets for similar energies. At higher energies, i.e., for 100, 150, and 250 eV, the CDW-EIS calculations underestimate the data by factors of about 4.0, 8.0, and 20, respectively. In contrast, for He targets the CDW-EIS model falls below the data only by factors of 4.0 at 200 eV and 6.0 at 300 eV, indicating a stronger deviation from the theory in the case of H_2 targets. The comparison of the data with the CDW calculations at higher energies can also be found from Figs. 4(d), 4(e), and 4(f). The CDW calculations, which reproduce the He data for backward angles very well for higher energies, now fall below the H_2 data by a factor of almost 1.7 at 100 eV, 2.4 at 150 eV, and 4.0 at 250 eV for the most backward angle measured. This might indicate the inadequacy of the approximation used to describe the molecular hydrogen wave function using the independent-electron model.

VI. ANGULAR DISTRIBUTIONS OF SDCS'S

The single-differential cross sections (SDCS's) $(d\sigma/d\Omega)$ were derived by performing numerical integrations over the electron energies, and are shown in Figs. 5 and 6 for He and H_2 targets, respectively. These data for all three targets, i.e., H, H_2, and He, are also tabulated in Table IV. The angular distribution clearly shows a maximum value at the smallest forward angle, and decreases slowly up to 60° for He target (Fig. 5). Beyond this angle the SDCS data fall very sharply, and then level off above 150°. The B1 calculations show an entirely different distribution, in which the cross sections are distributed almost symmetrically in the forward and backward angles. The calculations predict a cross section that is a factor of 3.0 smaller than the measured one at 15°, and over-

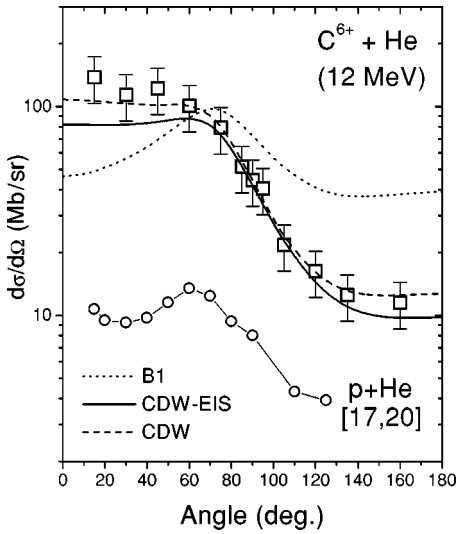

FIG. 5. The angular distributions of single-differential cross sections for $C^{6+}+$He (1 MeV/u, $v_p=6.35$). The different calculations are also shown by solid (CDW-EIS model), dashed (CDW model), and dotted (B1 model) lines. The circles joined by lines represent the SDCS for $p+$He at the same projectile velocity, and are taken from Refs. [17,20].

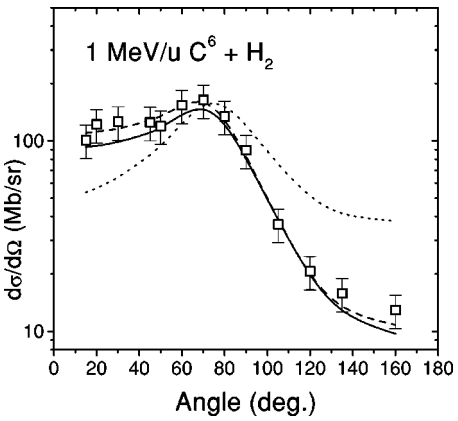

FIG. 6. The angular distributions of single-differential cross sections for H_2 targets. The different calculations are also shown by solid (CDW-EIS model), dashed (CDW model), and dotted (B1 model) lines.

estimates for large backward angles by almost the same factor. The two-center effect causes this enhancement in the forward angles, and a depletion in the large angles compared to the B1 prediction. The CDW-EIS prediction also falls slightly lower than the data in the case of small forward angles, underestimating them by about 30–70 %, but the calculations reproduce the data for the rest of the angles. The CDW model reproduces almost all the data points, giving very good agreement with the entire angular distribution. A similar comparison holds good for the SDCS data of H_2 targets as shown in Fig. 6. The CDW-EIS results fall about 20–30 % below the measured data at the extremely forward and backward angles, whereas the CDW model provides the best agreement while the B1 results are entirely different from the observed cross sections. The difference in the shape of the distributions for the He and H_2 targets, especially in the forward angles, is to be noted, since the peaklike structure around 70° in the case of H_2 is missing in the distribution for He targets. The peaking at about 70° is also observed in collisions with H targets, as discussed in paper I. The difference in the peak shapes for He and H_2 (or H) is due to the different Compton profiles for these molecules and the binary nature of the collisions. To compare the distributions (for same target atom) with similar data in proton collisions, in Fig. 5 we plot the SDCS's (circles joined by lines), for $p+$He at the same beam velocity ($v=6.35$), for which the perturbation strength is quite small ($S_p=0.16$) (taken from Refs. [17,20]). It is obvious that in this case, i.e., in collisions with light particles, the distribution peaks at 60°, and falls at small forward angles as well as large backward angles. The difference in the shape of the distributions in the case of heavy-ion collisions compared to that for proton collisions could arise due to the two-center effect, which is stronger for a heavy ion projectile for which $S_p \sim 1.0$.

It is obvious that the finer details of the energy and angular distributions of electron DDCS's in collisions with He or H_2 are better reproduced by the CDW calculations compared to the CDW-EIS calculations, as also observed in collisions with atomic hydrogen target (see paper I). This shows that a more detailed description of the ionization mechanism cannot be made without considering the electron as moving in a two-center field created by the heavy particles during the entire time of collision. In the CDW-EIS model, as mentioned earlier, the two-center character is emphasized mostly in the outgoing channel. Thus the present results show that better agreement and finer details on the DDCS's can only be achieved by including the two-center dynamics of the electron in the incoming path of the collision, as is done in the CDW model. These observations are similar for all three targets studied i.e., H, H_2, and He.

VII. TOTAL CROSS SECTIONS AND SCALING RULE

The total cross sections are also derived by integrating the angular distributions of the SDCS's over the whole angular range. The measured cross sections for He atoms is 679 Mb, which is in excellent agreement with the earlier observations by Shinpaugh *et al.* [21], who measured the total cross section to be 668 Mb for the same collision system. The calculated values are 777 Mb (B1 model), 595 Mb (CDW-EIS model), and 687 Mb (CDW model). The CDW model pro-

TABLE III. Same as in Table I, except for C^6+H_2.

θ, ε	2 eV	10 eV	30 eV	50 eV	80 eV	100 eV	150 eV	200 eV	250 eV	300 eV
15°	5.30	2.58	0.72	0.257	0.081	0.0374	0.0164	0.0088	0.0073	
20°	5.45	4.93	0.33	0.102	0.058	0.0207	0.0108			
30°	7.14	4.93	1.03	0.367	0.120	0.073	0.0267	0.0137	0.0069	
45°	6.13	5.00	1.15	0.445	0.169	0.107	0.0446	0.023	0.013	
50°	5.42	4.50	1.11	0.47	0.195	0.132	0.0596	0.0359	0.026	
60°	5.42	5.05	1.38	0.662	0.316	0.214	0.119	0.083	0.063	
70°	5.42	5.19	1.53	0.81	0.436	0.328	0.175	0.120	0.084	
80°	4.21	4.05	1.30	0.70	0.337	0.228	0.0922	0.0388		
90°	4.19	3.20	0.91	0.368	0.124	0.068	0.0146	0.00448	0.0015	
105°	2.77	1.64	0.204	0.0540	0.01182	0.00557	0.00137	4.54E-4		
120°	2.28	0.95	0.066	0.0159	0.00419	0.00206	5.28E-4	3.14E-4	1.6E-4	
135°	1.93	0.77	0.041	0.0107	0.00325	0.00137	6.5E-4	2.33E-4	1.34E-4	5.22E-5
160°	1.16	0.79	0.035	0.0095	0.00227	0.00127	4.82E-4	1.4E-4	1.1E-4	3.4E-5

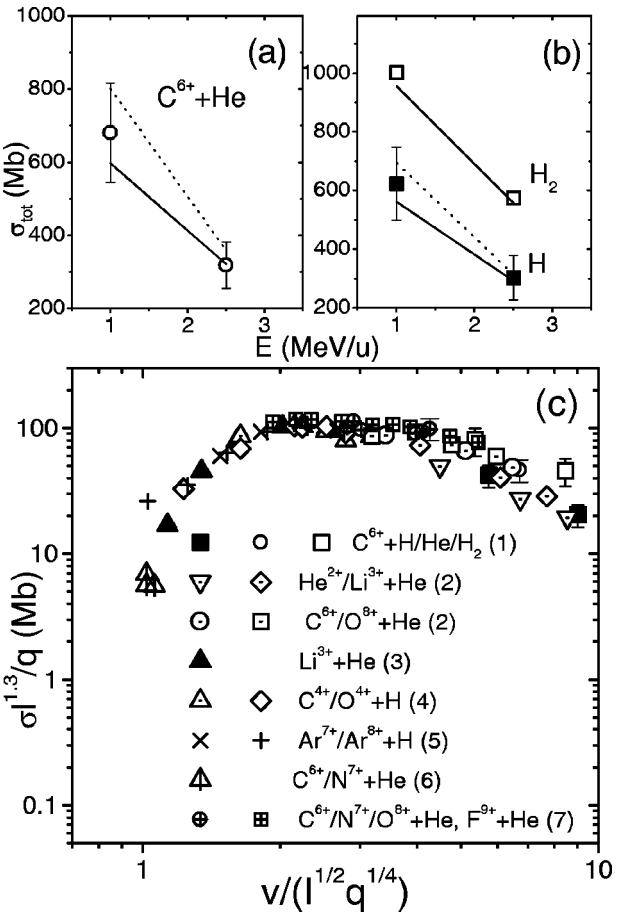

FIG. 7. The total ionization cross sections for $C^{6+}+He$ (a) and $C^{6+}+H_2$ and $C^{6+}+H$ (b) (paper I and Refs. [22,3]) at two collision energies. The scaled cross section vs the scaled velocity. The different sets of data are taken from the following references: (1) present and [22,3], (2) [27], (3) [26], (4) [25], (5) [24], (6) [18], and (7) [21].

vides the closest to the experimental value (within about 1%). In the case of H_2 molecules these values are 1001 Mb (measured), 907 Mb (CDW-EIS model), and 992 Mb (CDW model), the CDW model being the closest to the data. The measured data are shown in Figs. 7(a) and 7(b) along with the different calculations. The data at 2.5 MeV/u are taken from our earlier measurements [3,22]. It may be noted that all three calculations reproduce the measured cross sections quite well. This clearly indicates that the total cross sections are not sensitive enough to test the finer details of the theories or mechanisms of ion-atom ionization such as two-center effects.

It was shown by Wu and co-workers [18,23] that the total ionization cross sections for ion-atom collisions for different targets (H and He) follow a scaling rule in the low- and intermediate-velocity regions. The scaled cross sections (σ_{sc}) for different targets and different projectiles with various charge states seem to fall on a universal line when plotted against the scaled velocity (v_{sc}) for v_{sc}, up to about 4 a.u. The scaled cross sections and velocity are defined, in terms of the ionization potential (I in a.u.) and charge states (q), as $\sigma_{sc}=\sigma I^{1.3}/q$ and $v_{sc}=v/(I^{1/2}/q^{1/4})$. The present studies along with our previous results for 2.5 MeV $C^{6+}+(H,H_2,He)$ targets can be used to check the proposed scaling rule up to $v_{sc}\approx 9.0$. We show such a plot in Fig. 7(c), in which we also include some of the published results on the ionization of H and He by different ions such as He, Li, C, O, and Ar with a variety of charge states. It can be seen that most of the data points seem to bunch together to follow a universal scaling rule, which also holds good at much lower scaled velocities, as shown by Wu and co-workers [18,23]. The data points used in Fig. 7(c) belong to different collision systems, as listed here: $C+(H,He,H_2)$ ($v=6.35$ and 10) [22,3], $(N^{7+},C^{6+})+He$ ($v=1.58$) [18], $Ar^{7+,8+}+H$ ($v=1.2$–3.2) [24], $(C^{4+},O^{4+}+H$ ($v=5$–10) [25], $Li^{3+}+He$ ($v=1.4$–3.2) [26], $(He^{2+},Li^{3+},C^{6+},O^{8+})+He$ ($v=5$–9) [27], and $(C^{6+},N^{7+},O^{8+},F^{9+})+He$ ($v=3.2$–9) [21].

TABLE IV. The single differential cross sections ($d\sigma/d\Omega$) in units of Mb/sr, measured at different angles, for 1-MeV/u $C^{6+}+(H,He,H_2)$. Typical errors are about 25%.

Angle	H_2	H	He
15°	100.8	58.8	138
20°	122	–	–
30°	126	–	113.5
45°	125.1	84.6	121.9
50°	119.8	75.1	–
60°	154	90.9	100.5
70°	164	110.9	–
75°	–	–	79
80°	134.5	–	–
85°	–	–	51.5
90°	89.3	59.4	44.3
95°	–	–	40.4
105°	36.5	20	21.7
120°	20.63	10.2	16.24
135°	15.8	8.1	12.5
160°	12.9	6.1	11.5

VIII. FORWARD-BACKWARD ASYMMETRY PARAMETER

The forward-backward asymmetry in electron emission can be quantitatively estimated by studying the asymmetry parameter [$\alpha(\varepsilon)$] as a function of electron energy ε. The angular asymmetry parameter is defined as [5]

$$\alpha(\varepsilon)=\frac{\mathcal{D}(0)-\mathcal{D}(\pi)}{\mathcal{D}(0)+\mathcal{D}(\pi)}, \tag{1}$$

where $\mathcal{D}(\theta)$ represents the measured DDCS at an emission angle θ. Although $\mathcal{D}(0)$ and $\mathcal{D}(\pi)$ were not measured, they could be deduced by extrapolating the angular distributions since the distributions vary smoothly near 0° and 180°. At present, we use the DDCS's at 15° and 160° to calculate $\alpha(\varepsilon)$ from experimental data as well as from theoretical cross sections. It is obvious that the limit of $\alpha\rightarrow 0$ denotes a symmetric distribution, and $\alpha\rightarrow 1$ signifies a large asymme-

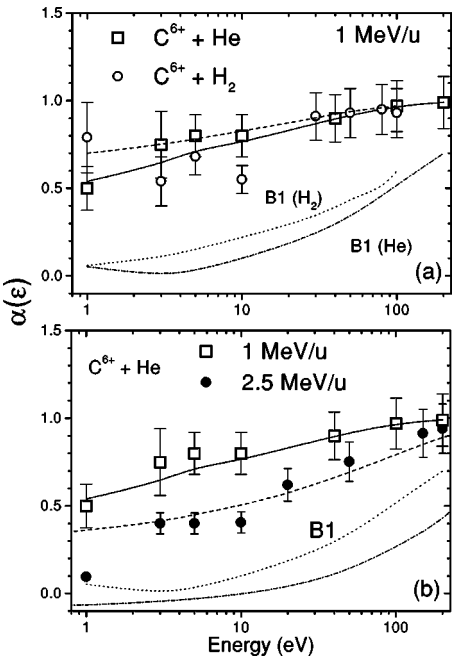

FIG. 8. (a) The forward-backward asymmetry parameter $[\alpha(\varepsilon)]$ as a function of electron energy (ε) for 1-MeV/u C6+ ions colliding on He (squares) and H_2 (circles) targets. The dashed (solid) line is the CDW-EIS calculations for the He (H_2) target. The B1 calculations are indicated in the figure. (b) The asymmetry parameter in the case of a $C^{6+}+He$ collision at two different beam energies, as indicated. The CDW-EIS calculations are shown as solid (1 MeV/u) and dashed (2.5 MeV/u) lines. The dotted and dash-dotted lines represent the B1 calculations at two different beam energies i.e., at 1 and 2.5 MeV/u, respectively.

try. In Fig. 8(a) we show $\alpha(\varepsilon)$ for He and H_2 targets as a function of the ε. It may be seen that $\alpha(\varepsilon)$ is very small $(\approx 0.5$ for $C^{6+}+He)$ in the zero-energy limit, and increases with the electron energy. It approaches 1.0 at about 100 eV. Fainstein *et al.* [5] showed that, apart from the TCE, the forward-backward asymmetry can also result if ionized electron moves in a non-Coulomb field, as in the case of any multielectron target (like He, in the present case). As a result the B1 model also shows a forward-backward asymmetry i.e., nonzero α, for $\varepsilon \rightarrow 0$. In the present case the α's from the B1 model are very small, indicating that the TCE is the most important contributor to the observed angular asymmetry of the low-energy electron emission. The CDW-EIS model (as well as the CDW model, which is not shown here) calculations give good agreement with the He data, but show some deviation from the data for H_2 in the lower energy region.

In Fig. 8(b) we display the comparison between the derived values of α for $C^{6+}+He$ collisions at two different beam energies, i.e., 1 and 2.5 MeV/u (obtained from Ref. [3]). It is clearly seen that the angular asymmetry is larger for low-energy collisions at all electron energies. However, part of the difference could be explained by the existing difference in the B1 model itself; the remaining part is due to the TCE which is stronger in the case of lower velocity collisions. The CDW-EIS calculations are in good agreement with both sets of data. The CDW model, however, provides results almost identical to the CDW-EIS model, and is therefore not shown.

IX. CONCLUSIONS

We have measured the absolute double-differential cross sections of low-energy (0.5–300 eV) electron emission for bare carbon ions colliding with helium and molecular hydrogen. The angular distributions are measured on a wide range of emission angles. The two-center effect is found to have a large influence on the forward-backward asymmetry of the electron DDCS's. A comparative study is presented for He and H_2 targets. The present studies (including the experiment with H target), covering three reduced velocities (i.e. $v/v_e = 4.7$, 5.9 and 6.35), provide a stringent test of the perturbative calculations based on B1 and continuum-distorted-wave approximations. The B1 calculations are shown to have failed largely to reproduce the large forward-backward asymmetry observed. The CDW-EIS model provides a reasonable agreement, although some discrepancies exist for electron emission in extreme forward and backward angles. The discrepancy is quite large in the case of H_2 targets compared to that for He targets. The CDW calculations are found to provide a better agreement with the data, especially at higher electron energies. The two-center electron emission is better represented by the CDW model compared to the CDW-EIS model. The forward-backward angular asymmetry was also studied for He and H_2, which provides a quantitative estimate of the two-center effect. The total ionization cross sections, derived for different target projectile combinations, are shown to follow a scaling rule, as recently proposed.

ACKNOWLEDGMENTS

This work was supported by the Division of Basic Energy of Chemical Sciences, Geosciences, and Biosciences Division, Office of Science, U.S. Department of Energy. One of us (L.C.T.) gratefully acknowledges the support provided by the JRM Laboratory, and L.G. gratefully acknowledges a grant of the J. Bolyai Research Scholarship.

[1] J. O. P. Pedersen, P. Hvelplund, A. Petersen, and P. Fainstein, J. Phys. B **24**, 4001 (1991).

[2] N. Stolterfoht, H. Platten, G. Schiwietz, D. Schneider, L. Gulyás, P. D. Fainstein, and A. Salin, Phys. Rev. A **52**, 3796 (1995).

[3] Lokesh C. Tribedi, P. Richard, Y. D. Wang, C. D. Lin, L. Gulyás, and M. E. Rudd, Phys. Rev. A **58**, 3619 (1998).

[4] D. S. F. Crothers and J. F. McCann, J. Phys. B **16**, 3229 (1983).

[5] P. D. Fainstein, V. H. Ponce, and R. D. Rivarola, J. Phys. B

24, 3091 (1991).
[6] L. Gulyás, P. D. Fainstein, and A. Salin, J. Phys. B **28**, 245 (1995).
[7] R. Moshammer, J. Ullrich, M. Unverzagt, W. Schmidt, P. Jardin, R. E. Olson, R. Mann, R. Dörner, V. Mergel, U. Buck, and H. Schmidt-Böcking, Phys. Rev. Lett. **73**, 3371 (1994).
[8] Lokesh C. Tribedi, P. Richard, Y. D. Wang, C. D. Lin, and R. E. Olson, Phys. Rev. Lett. **77**, 3767 (1996).
[9] Y. D. Wang, Lokesh C. Tribedi, P. Richard, C. L. Cocke, V. D. Rodríguez, and C. D. Lin, J. Phys. B **29**, L203 (1996).
[10] Lokesh C. Tribedi, P. Richard, Y. D. Wang, C. D. Lin, R. E. Olson, and L. Gulyás, Phys. Rev. A **58**, 3626 (1998).
[11] R. E. Olson, C. J. Wood, H. Schmidt-Böcking, R. Moshammer, and J. Ullrich, Phys. Rev. A **58**, 270 (1998).
[12] W. E. Meyerhof, H.-P. Hülskötter, Q. Dai, J. H. McGuire, and Y. D. Wang, Phys. Rev. A **43**, 5907 (1991); Y. D. Wang, J. H. McGuire, and R. D. Rivarola, *ibid.* **40**, 3673 (1989).
[13] E. Krishnakumar, Bhas Bapat, F. A. Rajgara, and M. Krishnamurthy, J. Phys. B **27**, L777 (1994); E. Krishnakumar and F. A. Rajgara, *ibid.* **26**, 4155 (1993).
[14] S. Cheng, C. L. Cocke, E. Y. Kamber, C. C. Hsu, and S. L. Varghese, Phys. Rev. A **42**, 214 (1990).
[15] D. E. Golden and H. W. Bandel, Phys. Rev. **138**, A14 (1965).
[16] D. E. Golden, H. W. Bandel, and J. A. Salerno, Phys. Rev. **140**, 40 (1966).
[17] M. E. Rudd, L. H. Toburen, and N. Stolterfoht, At. Data Nucl. Data Tables **18**, 413 (1976).
[18] W. Wu, E. F. Deveney, S. Datz, D. D. Desai, H. F. Krause, J. M. Sanders, C. R. Vane, C. L. Cocke, and J. P. Giese, Phys. Rev. A **53**, 2367 (1996).
[19] A few typographical errors were detected in our earlier data table (Table I in Ref. [3]) in which the electron DDCS's for 2.5-MeV/u C^{6+} + He were tabulated. The corrected numbers at two different angles ($\theta = 135°$ and 160° and $\varepsilon = 210-300$ eV) are shown in Table II. Accordingly, the angular distribution of the corrected DDCS at 300 eV, which is slightly different from that shown earlier in Fig. 4 of Ref. [3], is plotted again in Fig. 3(g).
[20] Steven T. Manson, L. H. Toburen, and N. Stolterfoht, Phys. Rev. A **12**, 60 (1975).
[21] J. L. Shinpaugh, J. M. Sanders, J. M. Hall, D. H. Lee, H. Schmidt-Boecking, T. N. Tipping, T. J. M. Zouros, and P. Richard, Phys. Rev. A **45**, 2922 (1992).
[22] Lokesh C. Tribedi, P. Richard, W. DeHaven, L. Gulyás, and M. E. Rudd, J. Phys. B **31**, L369 (1998).
[23] W. Wu, C. L. Cocke, J. P. Giese, F. Melchert, M. L. A. Raphaelian, and M. Stockli, Phys. Rev. Lett. **75**, 1054 (1995).
[24] M. B. Shah and H. B. Gilbody, J. Phys. B **16**, 4395 (1983).
[25] M. B. Shah and H. B. Gilbody, J. Phys. B **14**, 2831 (1981).
[26] M. B. Shah and H. B. Gilbody, J. Phys. B **18**, 899 (1985).
[27] H. Knudsen, L. H. Andersen, P. Hvelplund, G. Astner, H. Cederquist, H. Danared, L. Liljeby, and K.-G. Rensfelt, J. Phys. B **17**, 3545 (1984).